Letter

Giant linear magnetoelectric effect at the morphotropic phase boundary of epitaxial $Sr_{0.5}Ba_{0.5}MnO_3$ films

Temuujin Bayaraa,[1] Yurong Yang,[2,3,4] Meng Ye,[5] and L. Bellaiche[1,2]

[1]*Physics Department, University of Arkansas, Fayetteville, Arkansas 72701, USA*

[2]*Institute for Nanoscience and Engineering, University of Arkansas, Fayetteville, Arkansas 72701, USA*

[3]*National Laboratory of Solid-State Microstructures and Collaborative Innovation Center of Advanced Microstructures, Department of Materials Science and Engineering, Nanjing University, Nanjing 210093, China*

[4]*Jiangsu Key Laboratory of Artificial Functional Materials, Nanjing University, Nanjing 210093, China*

[5]*Department of Physics, Tsinghua University, Beijing 100084, China*

(Received 3 August 2020; accepted 1 February 2021; published 15 February 2021)

First-principles calculations are conducted to compute linear magnetoelectric coupling coefficients in epitaxial (001) $Sr_{0.5}Ba_{0.5}MnO_3$ films. A large enhancement of different linear magnetoelectric elements is found in a strained-induced morphotropic phase boundary region. Such enhancement is demonstrated to originate from the behavior of the dielectric susceptibility, thanks to a simple phenomenological model that is presently shown to be relevant and accurate. This work can thus provide a promising approach towards designing highly desired single-phase multiferroic with a colossal magnetoelectric conversion.

DOI: 10.1103/PhysRevB.103.L060103

In the last two decades, the search for magnetoelectric multiferroics possessing a strong coupling between their ferroelectric and magnetic properties has attracted great interest [1,2], for technological and fundamental purposes. The understanding of the underlying mechanism behind magnetoelectric coupling is a crucial line of research. It can lead to the development of potentially innovative technologies that would make possible a control of electrical properties by a magnetic field or, conversely, of magnetic quantities by an electric field. Examples include spintronic devices, multistate memory devices, and the long-searched electric-writing magnetic-reading random access memory, etc. [3–6].

However, magnetoelectric coupling in single-phase multiferroics is usually weak or only significant at very low temperatures [7], which is one of the biggest obstacles for technological applications. Hence, the research on multiferroic systems and approaches with a large magnetoelectric coupling is receiving considerable attention [8–13]. Among the various families of multiferroics, ABO_3 perovskite oxides are under extensive scrutiny and, for instance, a strong phase-change magnetoelectric response has been predicted in the $BiFeO_3$-$BiCoO_3$ solid solutions by a first-principles investigation [14]. It was found to be associated with the transition between two structural polymorphs of rhombohedral *R*3*c* and tetragonal *P*4*mm* symmetries. Electric-field driven transition between these two polymorphs leads to the rotation of the easy magnetic axis with a change in direction and magnitude of spontaneous polarization. Experimental verification of the polarization rotations with composition and temperature was then realized in the $BiCo_{1-x}Fe_xO_3$ system adopting the monoclinic *Cm* symmetry [15]. Moreover, magnetoelectricity at a region of so-called morphotropic phase boundary (MPB), for which the systems exhibit several different phases, was achieved experimentally in the chemically designed $BiFeO_3$-$BiMnO_3$-$PbTiO_3$ ternary system [16,17] and $(1-x)BiTi_{(1-y)/2}Fe_yMg_{(1-y)/2}O_3$-$xCaTiO_3$ compound [18]. Such results suggest a promising approach to achieve a large magnetoelectric coupling in multiferroics using the nature of MPB. Moreover, enhancement of magnetoelectric response was predicted to be linked with the softening of the lattice by a recent study [19]. It is thus timely to wonder if it is possible to induce large magnetoelectricity in simpler materials and in a simpler way [20], but still using this concept of MPB—that is known to make the lattice soft. Such a hypothetical possibility would make applications more feasible. Knowing the precise physical quantity responsible for a large enhancement of magnetoelectricity is also of fundamental interest.

Interestingly, in previous work, a *strain-induced* MPB bridging two known tetragonal and orthorhombic states, via a monoclinic state with the continuous rotation of the spontaneous polarization, was found in multiferroic $Sr_{0.5}Ba_{0.5}MnO_3$ (SBMO) films [21]. In this letter, we therefore decided to use a first-principles approach to study, and understand, magnetoelectricity in SBMO films, in order to test the general strategy of employing strain engineering to induce a large enhancement in magnetoelectric coupling in the MPB region. Large enhancement of different linear magnetoelectric coefficients is indeed found here. It is further demonstrated to be related to the strain-induced behavior of the dielectric susceptibility.

We focus here on epitaxial (001) $Sr_{0.5}Ba_{0.5}MnO_3$ (SBMO) films for which we adopt a rocksalt ordering between its Ba and Sr atoms. A $\sqrt{2} \times \sqrt{2} \times 2$ supercell having 20 atoms is chosen to accommodate the *G*-type antiferromagnetic (*G*-AFM) configuration. We also checked another chemically ordered structure, which is the one indicated in Ref. [21], and

found similar qualitative results regarding the enhancement of the linear magnetoelectric coefficient for some epitaxial strains; details are demonstrated in the Supplemental Material [22]. To mimic (001) epitaxial films experiencing a strain induced by any prechosen in-plane lattice parameter a_{ip}, the in-plane lattice vectors are frozen during the simulations with their length being directly proportional to a_{ip}. All the other structural degrees of freedom, including the out-of-plane lattice vector and atomic positions, are allowed to relax in order to minimize the total energy until Hellmann-Feynman forces are less than 2 μeV/Å on each ion (this strict requirement is imposed in order to be able to have a mostly linear change of the polarization as a function of an external magnetic field). SBMO films with a_{ip} ranging between 3.81 and 3.98 Å are practically studied here, adopting the *G*-AFM configuration since it is the lowest magnetic state for this range of a_{ip} [21].

We perform density functional theory (DFT) calculations, as implemented in the Vienna *ab initio* simulation package (VASP) [23] and using the Perdew-Burke-Ernzerhof (PBE) + U + J functional [24,25]; the details being as in Ref. [21] with Hubbard U and Hund J corrections on Mn atoms chosen to be 3 and 1 eV, respectively [26]. The electric polarization is calculated using the Berry-phase method [27], and structural and magnetic space groups are identified using the FINDSYM software [28]. The linear magnetoelectric coupling coefficient is computed by applying an external magnetic field on the magnetic enthalpy energy [29] and details can be found in the Supplemental Material [22]. This method was found to be valid and accurate in various systems [29–32]; for example, for the typical prototype of magnetoelectric Cr_2O_3, the linear magnetoelectric coupling coefficient was computed to be 1.45 ps/m [32] which is in good agreement with experimental result of 1.58 ps/m [33]. Note that the linear magnetoelectric coupling in our study includes both ionic and electronic contributions. In this study, all calculations are performed under external magnetic fields ranging from 0 to 30 T, including spin-orbit coupling. Furthermore, we also calculated vibrational properties by the linear response method as implemented in the PHONOPY code [34], the dielectric susceptibility is calculated by density functional perturbation theory implemented in VASP, and the magnetic susceptibility is determined by analyzing the slope of change in the total magnetic moment when an external magnetic field is applied.

First, let us concentrate on the magnetic and physical properties of SBMO films throughout the studied epitaxial strain. As reported before [21] and as recalled in Fig. 1(a) (that shows the total energy as a function of the a_{ip} for the *G*-AFM magnetic configuration), SBMO films go through two structural phase transitions, via the MPB bridging two high-symmetry states (tetragonal and orthorhombic). In the a_{ip} regime below 3.869 Å, SBMO films favor the tetragonal *I*4*mm* state with an electric polarization lying along the pseudocubic [001] direction and are found to have an easy magnetic axis along the in-plane *b* axis (pseudocubic [110] direction), therefore resulting in the magnetic point group being $m'm2'$. On the other hand, for the a_{ip} regime above 3.9 Å, SBMO films favor the orthorhombic *Imm*2 state with an electric polarization pointing along the *b* axis and a magnetic easy axis lying along the in-plane *a* axis (pseudocubic [1–10] direction), also

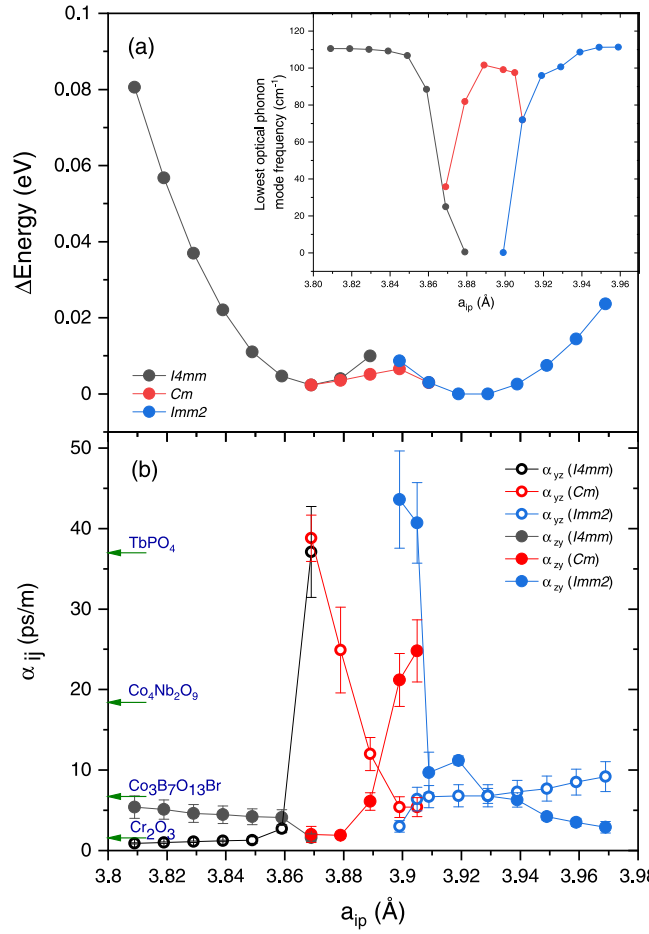

FIG. 1. Properties of SBMO films as a function of their in-plane lattice parameter in the *I*4*mm*, *Cm*, and *Imm*2 structural states: (a) the total energy, and (b) linear magnetoelectric coupling components. The zero of energy in (a) corresponds to the lowest energy structure, having a_{ip} = 3.919 Å. The inset in (a) shows the lowest optical frequency at the Γ point as a function of the in-plane lattice parameter. α values of four representative materials are also indicated by arrows on the vertical axis of (b) [37,38].

yielding a magnetic point group of $m'm2'$. Moreover, in the bridging monoclinic *Cm* state with its electric polarization direction rotating from the out-of-plane pseudocubic [001] axis to the in-plane [110] direction as a_{ip} increases [21], the easy magnetic axis in SBMO films is found to be rotating from the *b* axis to the *a* axis as a_{ip} increases, with a corresponding magnetic space group *m*. Note that the inset of Fig. 1(a) shows the computed lowest optical frequency at the Γ point as a function of a_{ip} [35]. Such frequency is found to drop sharply near the phase transition points, indicating that the high-symmetry tetragonal and orthorhombic structures are becoming dynamically unstable and thus wish to transition to the lower-symmetry associated with the monoclinic state within the MPB region.

Let us now pay attention to the linear magnetoelectric coupling tensor α_{ij}. According to the $m'm2'$ magnetic space group [11], only two nonzero and different α tensor components should exist: they are α_{yz} and α_{zy} [36]. These components are displayed in Fig. 1(b) as a function of the a_{ip}. Techni-

cally, α_{yz} is determined by applying different magnitudes of a magnetic field along the c axis and analyzing the slope of the change in the polarization results along the b axis and a axis in tetragonal and orthorhombic states, respectively. Similarly, the value of α_{zy} is determined by extracting the change in the polarization along the c axis when applying different magnitudes of a magnetic field along the b axis and a axis in tetragonal and orthorhombic states, respectively. In the monoclinic state, α_{yz} and α_{zy} values are determined by the same method as in tetragonal and orthorhombic phases but with the y axis varying from the b axis (smaller a_{ip}) to the a axis (larger a_{ip}) when the magnetic easy axis changes around a_{ip} of 3.89 Å (recall that the magnetic easy axis rotates within the MPB). The error bars in Fig. 1(b) represent the associated uncertainty of the slope of the linear fitting when studying the change in polarization as a function of an external magnetic field, in these three phases. One can clearly see that the α_{zy} values in the orthorhombic $Imm2$ state increase sharply when decreasing the a_{ip} near the structural phase transition point to the Cm phase, and then strongly decrease within this monoclinic Cm state when further reducing a_{ip}. Similarly, α_{yz} experiences a sharp increase within Cm when decreasing the a_{ip} until approaching the transition to the tetragonal $I4mm$ phase and then is significantly reduced within this $I4mm$ state when the system is further compressively and epitaxially strained. Consequently, α_{yz} and α_{zy} cross each other around a_{ip} of 3.895 Å within the monoclinic state. Figure 1(b) further reveals a remarkable quantitative result of our simulations, namely the linear magnetoelectric couplings in SBMO films can be practically enhanced to reach values as large as 40 ps/m near the phase transition points. To put our results in perspective, we report several representative materials that have been discovered to have giant magnetoelectric coupling and indicate their values in Fig. 1(b): (i) $TbPO_4$ single crystal is the strongest known magnetoelectric material with an α value of about 37 ps/m [37]; (ii) $Co_4Nb_2O_9$ with an α about 18.4 ps/m [38]; (iii) $Co_3B_7O_{13}Br$ with an α about 6.7 ps/m [37]; and (iv) the typical prototype of magnetoelectric, which is Cr_2O_3, with α about 1.58 ps/m [33]. The linear magnetoelectric coefficients of SBMO films within a certain range of epitaxial strains can thus be comparable to the strongest known α's (note that our computed values are at 0 K while the 37-ps/m value of $TbPO_4$ has been achieved at 2 K). Our computed a_{ip} of films with the highest α coefficients are 3.869 and 3.909 Å which, after rescaling by the expected overestimation of 0.34% mentioned above, become 3.856 and 3.896 Å, respectively. Interestingly, these corrected lattice constants are very close to the pseudocubic lattice constants of $NdGaO_3$ [39] and $SrTiO_3$ [40], that are 3.86 and 3.905 Å, respectively. Such a fact suggests that the growth of SBMO films on these substrates should lead to the observation of our predicted giant α values.

Let us now try to understand the results of Fig. 1(b), in general, and the origin of the large values of the linear magnetoelectric coefficients. For that, we recall the conclusion of analytical derivations, using a phenomenological model [41], and predicting that the linear magnetoelectric coupling coefficient can be expressed as

$$\alpha_{ij} = \alpha_{ij}^{(1)} + \alpha_{ij}^{(2)}, \quad \text{with} \quad \alpha_{ij}^{(1)} = -\sum\nolimits_{pqr} g_{pqr}\chi_{pi}^{p}L_r\chi_{qj}^{M} \quad \text{and} \quad \alpha_{ij}^{(2)} = -4\varepsilon_0\sum\nolimits_{pq}\lambda_{pq}P_p\chi_{pi}^{p}M_q\chi_{qj}^{M}, \tag{1}$$

where λ_{pq} and g_{pqr} are second and third rank tensors that are dependent on the material by itself but also on the symmetry of the crystal. M_q, P_p, and L_r are the q, p, and r component of magnetization, polarization, and the antiferromagnetic vector, respectively. ε_0 is the dielectric permittivity of vacuum, and χ_{pi}^{p} and χ_{qj}^{M} are elements of the dielectric and magnetic susceptibility tensors, respectively. Note that the use of $\alpha_{ij}^{(2)}$ (in addition to $\alpha_{ij}^{(1)}$) stems from the fact that we numerically found a weak ferromagnetism ($M_y = 0.0001\mu_B$, $M_z = 0.002\mu_B$, and $M_z = 0.005\mu_B$ in the $I4mm$, Cm, and $Imm2$ states, respectively) along with a strong G-AFM configuration in SBMO films. Such findings are consistent with the magnetic space groups of SBMO films, $m'm2'$ and m, which allows weak ferromagnetism [37].

Figures 2(a)–2(f) show the DFT-computed α_{yz} and α_{zy} values as a function of a_{ip} in Cm, $I4mm$, and $Imm2$ phases. Such figures also report the corresponding fitted values [42] using Eqs. (1) for which we employ the dielectric and magnetic susceptibility tensor components and polarization values as computed from DFT (and that are depicted in Fig. 3) and allow λ_{yz}, λ_{zy}, g_{zxy}, and g_{yxz} to be free fitting parameters [since α is linearly dependent on these parameters according to Eqs. (1), a new theoretical development is highly encouraged in order to directly calculate these second and third rank tensors]. Note that, since there is a weak ferromagnetism M_y but along the y direction in $I4mm$, $\alpha_{yz} = \alpha_{yz}^{(1)}$ in $I4mm$. Similarly, $\alpha_{zy} = \alpha_{zy}^{(1)}$ in Cm and $Imm2$ because only M_z is nonzero in these two states. Interestingly, Fig. 2 shows that the DFT-obtained linear magnetoelectric coefficients are well fitted by Eqs. (1), which demonstrate their relevance and applicability. As also revealed by Figs. 2(a), 2(d), and 2(f), using both terms, rather than only the first one, of Eqs. (1) typically allows us to better reproduce the computed linear magnetoelectric coupling coefficients, α_{zy} in $I4mm$, α_{yz} in Cm, and α_{yz} in $Imm2$, as also found for the case of $BiFeO_3$ [41]. However, such better agreement has to be taken with a grain of salt, once considering the error bars of the DFT values.

Since Figs. 2(a)–2(f) demonstrate that Eqs. (1) reproduce quite well the DFT-computed α_{yz} and α_{zy} values, one "just" has to look in detail into the strain-induced behaviors of the dielectric and magnetic susceptibility tensors components, in order to understand large values of magnetoelectricity. For that, Fig. 3(a) shows the calculated dielectric susceptibility tensor components χ_{yy}^{P} and χ_{zz}^{P} of SBMO films throughout the studied epitaxial strain range (with the definition of the y and z axes having been introduced above). χ_{yy}^{P} and χ_{zz}^{P} adopt large values at the $I4mm$ to Cm and Cm to $Imm2$ phase transition points, respectively, which is also in line with the softening of the zone-center optical frequency displayed in the inset

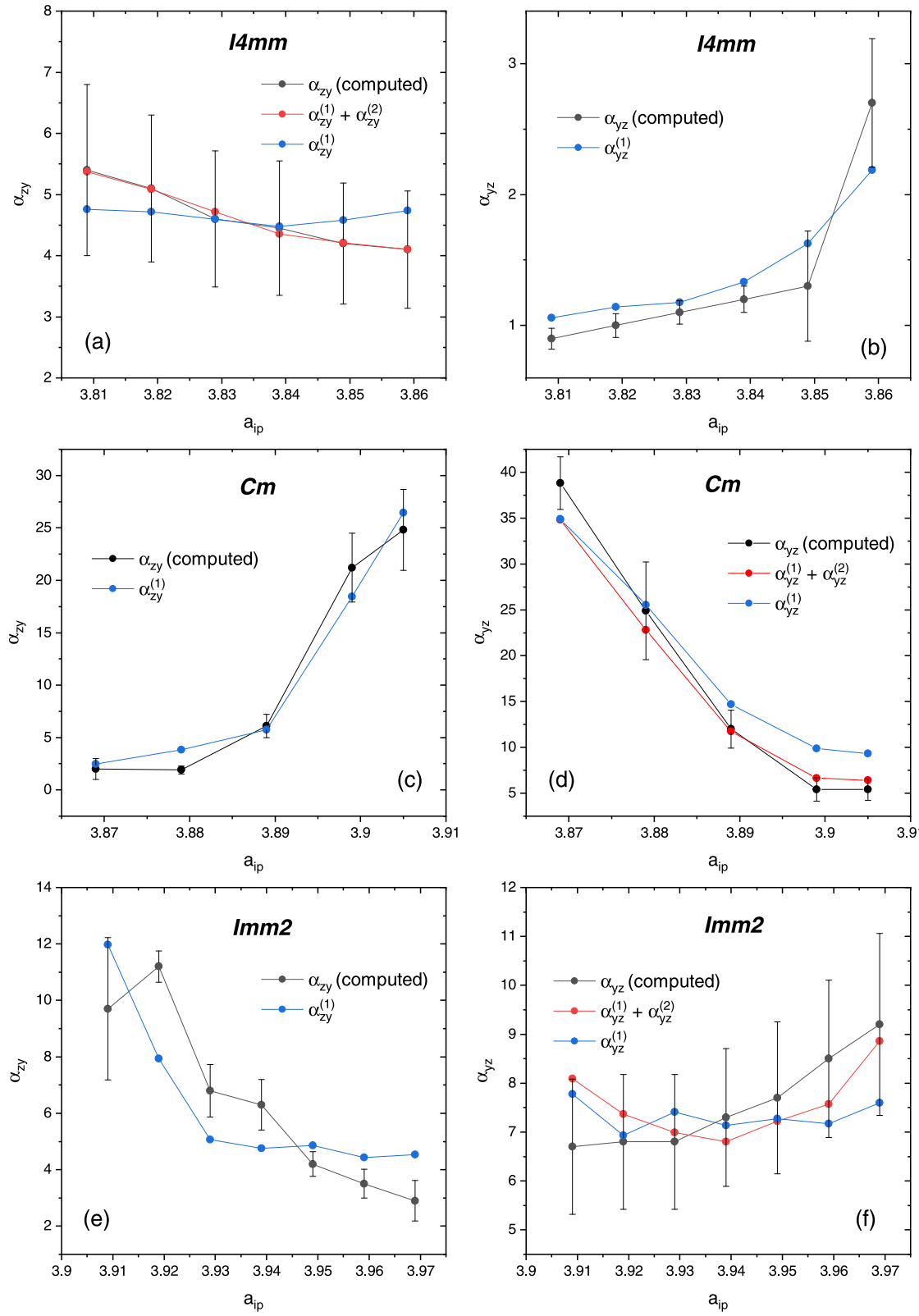

FIG. 2. Computed linear magnetoelectric coupling coefficients (α_{yz} and α_{zy}) as a function of a_{ip} with its corresponding fitted values ($\alpha_{yz} = \alpha_{yz}^{(1)} + \alpha_{yz}^{(2)} = -g_{zxy}\chi_{yy}^{P}L_x\chi_{zz}^{M} - 4\varepsilon_0\lambda_{yz}P_y\chi_{yy}^{P}M_z\chi_{zz}^{M}$ and $\alpha_{zy} = \alpha_{zy}^{(1)} + \alpha_{zy}^{(2)} = -g_{yxz}\chi_{zz}^{P}L_x\chi_{yy}^{M} - 4\varepsilon_0\lambda_{zy}P_z\chi_{zz}^{P}M_y\chi_{yy}^{M}$) using Eqs. (1) in the $I4mm$, Cm, and $Imm2$ phases.

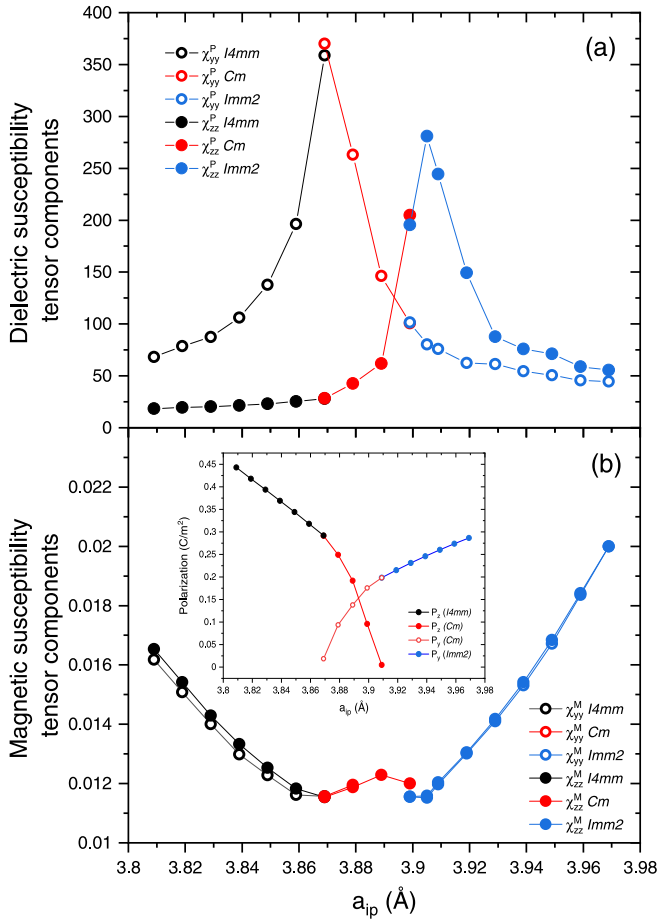

FIG. 3. Dielectric (a) and magnetic susceptibility (b) tensor components of epitaxial (001) SBMO films as a function of a_{ip} in *I*4*mm*, *Cm*, and *Imm*2 states. The inset in (b) shows the polarization values of SBMO films as a function of a_{ip}.

of Fig. 1(a)—while χ^M_{zz} and χ^M_{yy} values adopt their minimum values at these transition points and remain mostly unchanged throughout the *Cm* phase [see Fig. 3(b) and calculation detail of χ^M_{zz} and χ^M_{yy} values demonstrated in the Supplemental Material [22]]. Consequently, and according to Eqs. (1), the large values of the α_{yz} of 38.8 ps/m and α_{zy} of 24.8 ps/m linear magnetoelectric coefficients reside in the large χ^P_{yy} and χ^P_{zz} near phase transitions, respectively. Note that it is known that many structural phase transitions associated with lattice softening result in the divergence of the dielectric susceptibility due to the softening of the force-constant matrix at the phase transition, and that such divergence is also consistent with the electrical polarization acquiring/annihilating some of its components [43]. In other words, Eqs. (1) tell us that one can design multiferroic materials with a high linear magnetoelectric coefficient when inducing structural transitions for which dielectric susceptibilities become large, as numerically confirmed here and as implied by previous works [19,41,44–47] [note that Eqs. (1) also imply that large linear magnetoelectricity can also be reached at magnetic phase transitions that are accompanied by a dramatic increase in the magnetic susceptibility, which is not the case in the present study].

Moreover, Fig. 3(a) further reveals that χ^P_{yy} in *Imm*2 and χ^P_{zz} in *I*4*mm* decrease when a_{ip} is larger than 3.91 Å and smaller than 3.86 Å, respectively. However, in contrast, α_{yz} in the *Imm*2 state and α_{zy} in the *I*4*mm* state are found to concomitantly increase at these a_{ip} regimes. This is related to the magnetic susceptibility and polarization. As a matter of fact, Fig. 3(b) shows the magnetic susceptibility tensor components χ^M_{yy} and χ^M_{zz} of SBMO films under epitaxial strain while its inset shows the polarization as a function of a_{ip}. As one can see, all magnetic susceptibility tensor components increase as a_{ip} decreases below 3.859 Å, and as a_{ip} increases above 3.909 Å. Moreover, P_z in *I*4*mm* and P_y in *Imm*2 also increase as a_{ip} decreases below 3.859 Å and increases above 3.909 Å, respectively. The increases in χ^M_{yy} and P_z in the *I*4*mm* state and of χ^M_{zz} and P_y in the *Imm*2 state are fully consistent with the corresponding increase in α_{zy} in the *I*4*mm* state and α_{yz} in the *Imm*2 state, according to Eqs. (1).

In summary, we have computed the linear magnetoelectric coupling coefficients of epitaxial (001) SBMO films as a function of their a_{ip} arising from substrates. In particular, we found a large enhancement of α_{yz} and α_{zy} values at the phase transition points from *I*4*mm* to *Cm* and *Imm*2 to *Cm* states, respectively. Such enhancements are found to be directly related to the sudden increase of the dielectric susceptibility at the phase transition points. Magnetic susceptibility was also determined to influence the linear magnetoelectric coupling, but for smaller linear magnetoelectric coefficients (thus, technically, the linear magnetoelectric coupling can also be enhanced with the increase in magnetic susceptibility such as the one found in ferromagnetic MPB [48]). Note that the effect of the interface with the substrate on the electronic, magnetic properties and magnetoelectric coupling coefficient is ignored in this study and it may be a topic of future study. We hope that our predictions help in further understanding magnetoelectric effects, in general, and bring attention to single-phase multiferroics with MPB, in particular, to achieve highly desired colossal magnetoelectric responses.

This work was supported by the Department of Energy, Office of Basic Energy Sciences, under Award No. DE-SC0002220. Y.Y. acknowledges support from the National Natural Science Foundation of China (Contract No. 11874207) and the National Key R&D Program of China (Grant No. 2020YFA0711504). We also acknowledge the DoD High Performance Computing Modernization Program (HPCMP) for providing access to the computational clusters.

[1] W. Eerenstein, N. D. Mathur, and J. F. Scott, Nature (London) **442**, 759 (2006).
[2] R. Ramesh and N. A. Spaldin, Nat. Mater. **6**, 21 (2007).
[3] M. Bibes and A. Barthélémy, Nat. Mater. **7**, 425 (2008).
[4] S. Fusil, V. Garcia, A. Barthélémy, and M. Bibes, Annu. Rev. Mater. Res. **44**, 91 (2014).
[5] M. M. Vopson, Crit. Rev. Solid State Mater. Sci. **40**, 223 (2015).

[6] S. Dong, J.-M. Liu, S.-W. Cheong, and Z. Ren, Adv. Phys. **64**, 519 (2015).

[7] D. Khomskii, Physics **2**, 20 (2009).

[8] D. Pantel, S. Goetze, D. Hesse, and M. Alexe, Nat. Mater. **11**, 289 (2012).

[9] R. O. Cherifi, V. Ivanovskaya, L. C. Phillips, A. Zobelli, I. C. Infante, E. Jacquet, V. Garcia, S. Fusil, P. R. Briddon, N. Guiblin, A. Mougin, A. A. Ünal, F. Kronast, S. Valencia, B. Dkhil, A. Barthélémy, and M. Bibes, Nat. Mater. **13**, 345 (2014).

[10] H. J. Zhao, W. Ren, Y. Yang, J. Íñiguez, X. M. Chen, and L. Bellaiche, Nat. Commun. **5**, 4021 (2014).

[11] A. Kumar, G. L. Sharma, R. S. Katiyar, R. Pirc, R. Blinc, and J. F. Scott, J. Phys.: Condens. Matter **21**, 382204 (2009).

[12] J. F. Scott, NPG Asia Mater. **5**, e72 (2013).

[13] D. M. Evans, A. Schilling, A. Kumar, D. Sanchez, N. Ortega, M. Arredondo, R. S. Katiyar, J. M. Gregg, and J. F. Scott, Nat. Commun. **4**, 1534 (2013).

[14] O. Diéguez and J. Íñiguez, Phys. Rev. Lett. **107**, 057601 (2011).

[15] K. Oka, T. Koyama, T. Ozaaki, S. Mori, Y. Shimakawa, and M. Azuma, Angew. Chemie Int. Ed. **51**, 7977 (2012).

[16] C. M. Fernández-Posada, H. Amorín, C. Correas, O. Peña, M. Algueró, and A. Castro, J. Mater. Chem. C **3**, 2255 (2015).

[17] C. M. Fernández-Posada, A. Castro, J.-M. Kiat, F. Porcher, O. Peña, M. Algueró, and H. Amorín, Nat. Commun. **7**, 12772 (2016).

[18] P. Mandal, M. J. Pitcher, J. Alaria, H. Niu, P. Borisov, P. Stamenov, J. B. Claridge, and M. J. Rosseinsky, Nature (London) **525**, 363 (2015).

[19] J. C. Wojdeł and J. Íñiguez, Phys. Rev. Lett. **105**, 037208 (2010).

[20] This simple way does not involve the mixing between three or more systems, and does not require us to apply electric fields, or change composition, to break the symmetry of the system towards lower-in-symmetry phases.

[21] T. Bayaraa, Y. Yang, H. J. Zhao, J. Íñiguez, and L. Bellaiche, Phys. Rev. Mater. **2**, 084404 (2018).

[22] See Supplemental Material at http://link.aps.org/supplemental/10.1103/PhysRevB.103.L060103 for the details on how the linear magnetoelectric coupling coefficient is computed and further information into how the polarization and magnetization of the (001) $Sr_{0.5}Ba_{0.5}MnO_3$ (SBMO) films respond to applied magnetic fields and the results of the linear magnetoelectric coupling coefficient of another chemically-ordered structure of SBMO films.

[23] G. Kresse and J. Furthmüller, Phys. Rev. B **54**, 11169 (1996).

[24] J. P. Perdew, K. Burke, and M. Ernzerhof, Phys. Rev. Lett. **77**, 3865 (1996).

[25] A. I. Liechtenstein, V. I. Anisimov, and J. Zaanen, Phys. Rev. B **52**, R5467 (1995).

[26] Note that, by comparing a_{ip} of both measurements [25] and calculations (using PBE + U + J functional with $U = 3$ eV and $J = 1$ eV) for bulk SBMO, we estimate an overestimation of about 0.34% for the lattice constants. Such small overestimation demonstrates the rather high accuracy of our calculations.

[27] R. D. King-Smith and D. Vanderbilt, Phys. Rev. B **47**, 1651 (1993).

[28] H. T. Stokes and D. M. Hatch, J. Appl. Cryst **38**, 237 (2005).

[29] M. Ye and D. Vanderbilt, Phys. Rev. B **89**, 064301 (2014).

[30] M. Ye and D. Vanderbilt, Phys. Rev. B **92**, 035107 (2015).

[31] H. Tian, L. Bellaiche, and Y. Yang, Phys. Rev. B **100**, 220103(R) (2019).

[32] E. Bousquet, N. A. Spaldin, and K. T. Delaney, Phys. Rev. Lett. **106**, 107202 (2011).

[33] E. Kita, K. Siratori, and A. Tasaki, J. Appl. Phys. **50**, 7748 (1979).

[34] A. Togo and I. Tanaka, Scr. Mater. **108**, 1 (2015).

[35] Note that the results displayed in the inset of the present Fig. 1(a) are obtained from the linear response method as implemented in the PHONOPY code [32] while the results shown in Fig. 3 of Ref. [20] are determined with the finite difference method implemented in VASP [21]. The two results provide, overall, similar outcomes with a less than 20 cm^{-1} difference in the magnitude of the frequencies. Some results are, however, slightly different between the two methods, such as the lowest optical frequencies at the Γ point slightly decreasing in Ref. [20] rather than slightly increasing in the current Letter in the *I*4*mm* phase when the in-plane lattice parameter decreases below 3.85 Å. We are confident that this latter behavior is more physical (since the polarization concomitantly increases), explaining why we trust more the results of PHONOPY here.

[36] Recall that the first index of these coefficients is associated with the component of the polarization while the second index refers to the component of the applied magnetic field $P_i = \alpha_{ij} H_j$, and further information is provided in the Supplemental Material [22].

[37] A. S. Borovik-Romanov, H. Grimmer, and M. Kenzelmann, Magnetic properties, in *International Tables for Crystallography Volume D: Physical Properties of Crystals*, edited by A. Authier (Springer, Dordrecht, 2013), pp. 139–145.

[38] Y. Fang, Y. Q. Song, W. P. Zhou, R. Zhao, R. J. Tang, H. Yang, L. Y. Lv, S. G. Yang, D. H. Wang, and Y. W. Du, Sci. Rep. **4**, 3860 (2014).

[39] G. F. Ruse and S. Geller, J. Cryst. Growth **29**, 305 (1975).

[40] M. Kawasaki, K. Takahashi, T. Maeda, R. Tsuchiya, M. Shinohara, O. Ishiyama, T. Yonezawa, M. Yoshimoto, and H. Koinuma, Science, **266**, 1540 (1994).

[41] S. Prosandeev, I. A. Kornev, and L. Bellaiche, Phys. Rev. B **83**, 020102 (2011).

[42] We have here $\alpha_{yz} = \alpha_{yz}^{(1)} + \alpha_{yz}^{(2)} = -g_{zxy}\chi_{yy}^{P} L_x \chi_{zz}^{M} - 4\varepsilon_0 \lambda_{yz} P_y \chi_{yy}^{P} M_z \chi_{zz}^{M}$ and $\alpha_{zy} = \alpha_{zy}^{(1)} + \alpha_{zy}^{(2)} = -g_{yxz}\chi_{zz}^{P} L_x \chi_{yy}^{M} - 4\varepsilon_0 \lambda_{zy} P_z \chi_{zz}^{P} M_y \chi_{yy}^{M}$.

[43] The creation/annihilation of the z component of the polarization can lead to a large χ_{zz}^{P}, while a large χ_{yy}^{P} can originate from the appearance/disappearance of the y component of the polarization.

[44] E. Bousquet and N. Spaldin, Phys. Rev. Lett. **107**, 197603 (2011).

[45] A. Edström and C. Ederer, Phys. Rev. Res. **2**, 043183 (2020).

[46] A. Edström and C. Ederer, Phys. Rev. Lett. **124**, 167201 (2020).

[47] A. Edström and C. Ederer, Phys. Rev. Mater. **2**, 104409 (2018).

[48] S. Yang, H. Bao, C. Zhou, Y. Wang, X. Ren, Y. Matsushita, Y. Katsuya, M. Tanaka, K. Kobayashi, X. Song, and J. Gao, Phys. Rev. Lett. **104**, 197201 (2010).